Research Article

Nucleation and mechanical enhancements in poly(butylene terephthalate) nanocomposites influenced by functionalized graphene oxide

Penghua Qian[1] · Yuxia Zhang[1] · Huiqin Mao[1] · Haixia Wang[1] · Haifeng Shi[1]

© Springer Nature Switzerland AG 2019

Abstract
Series of poly(butylene terephthalate) (PBT) nanocomposites are fabricated with polyethylene glycol methacrylate (PEGMA)-functionalized graphene oxide (GO) nanofillers (G-P) as the interfacial modifiers. PBT/G-P nanocomposites demonstrate good compatibility and interfacial interaction based on the uniform dispersed G-P nanofillers influenced by the grafted PEGMA chains. Crystallization behavior and nucleation density of PBT matrix get an increase and show a maximum at 1.5 wt% G-P nanofillers. Tensile strength and modulus of PBT/G-P nanocomposites first increase and then decrease with the varied G-P contents from 0.1 to 3.0 wt%, indicating the overloaded nanofillers impact the stress transfer. Against PBT/GO nanocomposites, PBT/G-P ones present 58% enhancement for the tensile strength, which is ascribed to the different interfacial compatibility afforded by the GO and G-P nanofillers. The present study demonstrates that it is a possible way to prepare high-performance PBT nanocomposites through the enhanced interfacial layer and nucleation behavior of polymer matrix.

Keywords Functionalized graphene oxide · Mechanical property · Nanocomposites · Poly(butylene terephthalate)

1 Introduction

Poly(butylene terephthalate) (PBT) is an important semicrystalline material, presenting very good dimensional stability, high heat resistance and chemical resistance [1], and so it has been used as engineering thermoplastics [2, 3], automobile [4], textile and composites [5, 6]. However, its low impact strength and mechanical property limit the further exploration of high-performance products [7, 8]. So, developing an improved performance with stable structure for PBT nanocomposites is highly desirable and interesting issue.

Typically, lots of studies are focused on the crystallization, thermal stability and mechanical property of PBT matrix, and some modifications have been done by blending organic polymers [9, 10] or incorporating inorganic nanofillers [11, 12]. Incorporating various inorganic nanofillers such as clay [13], halloysite [14] and carbon nanotubes [15, 16] into PBT matrix, the crystallization and nucleation behavior is greatly improved in light of the heterogeneous nucleation effect. Espinoza-Martinez [17] compared the nucleation mechanism of poly(ethylene terephthalate) (PET), poly(butylene terephthalate) (PBT) and poly(ethylene naphthalate) (PEN) influenced by single-wall carbon nanotubes (SWNTs), and they found a helical morphology for PET/SWNTs, PEN/SWNTs and a lobular one for PBT/SWNTs, which is ascribed to the π-π interactions and the chirality of nanotubes. Meanwhile, Tallury and Pasquinelli [18] also simulated the interface between SWCNTs and polymer chains with semiflexible and stiff backbones, and polymers with stiff and semiflexible backbones tended to wrap around the SWCNT. Although the nanofillers show a contribution to the nucleation and crystallization process of polymer matrix, the

✉ Haifeng Shi, haifeng.shi@gmail.com | [1]Tianjin Key Laboratory of Advanced Fiber and Energy Storage, School of Material Science and Engineering, Tianjin Polytechnic University, Tianjin 300387, China.

SN Applied Sciences (2019) 1:443 | https://doi.org/10.1007/s42452-019-0466-8

Received: 30 January 2019 / Accepted: 8 April 2019 / Published online: 10 April 2019

worse dispersion and compatibility limits the preparation of high-performance composites [7, 19–21]. Therefore, the nanofillers functionalized or grafted by polymer chains are beneficial to enhance the compatibility and the orientation state through the formed interfacial molecular layer with polymer matrix [22–24].

Through improving the dispersion state of nanofillers, the thermal stability and mechanical properties of polymer matrix greatly are enhanced. Chisholm et al. [25] prepared a highly exfoliated montmorillonite/PBT nanocomposites, giving 27% increased Young's modulus, which is contributed from the electrostatic interaction between clay particles and matrix. By changing the dispersion of CNT, PBT composites exhibit a nano-enhancement effect [7], and 35.1% increased tensile strength and 21.7% tensile modulus at 2.0 wt% loading of CNT are realized. Broza [6] reported a 29% increased tensile strength at 0.1 wt% SWNTs; however, at 0.2 wt% loading both the tensile strength and the crystallinity show a decrement. Li et al. [26] reported an 88% increased tensile modulus for PBT/graphene composites, followed by an improved thermal stability influenced by graphene nanosheets. In addition, by introducing 4.0 wt% graphene oxide (GO), Bian et al. [20] found a serious aggregation of GO nanosheets, indicating an overloading content will decrease the dispersion state into composites. Meanwhile, by incorporation of a highly reduced graphene oxide (RGO) into cyclic PBT matrix [27], a supernucleation role of RGO nanoflakes to PBT matrix is demonstrated. Additionally, the serious aggregation of bulky carbon-based nanofillers at high content also is a major problem to limit the development of polymer nanocomposites. Thus, improving the interfacial compatibility between nanofillers and polymer matrix demonstrates a good choice to explore the high-performance polymer nanocomposites. In our previous study [28], by introducing (3-aminopropyl) trimethoxysilane functionalized RGO nanofillers into polyimide matrix, a good reinforced mechanical and thermal property is shown, which is ascribed to the enhanced interfacial interaction and the good dispersion behavior RGO nanosheets. Similarly, Zhang and co-workers [29] also reported the improved mechanical behavior and thermal stability of polyurethane/epoxy resin composites after incorporation of (3-aminopropyl) trimethoxysilane-modified rGO nanosheets. That is to say, the functionalized nanofillers are helpful to increase the interfacial compatibility with the host matrix, and the stress-transfer process is greatly enhanced in light of the molecular chain entanglement and the interfacial action. Herein, in this paper, poly (ethylene glycol) methacrylate (PEGMA) monomer, a similar chain structure with PBT matrix, is grafted onto GO surface by redox polymerization process under the catalysis of ceric ammonium nitrate (CAN). Obvious nucleation and mechanical enhancement in PBT nanocomposites are demonstrated by the incorporated PEGMA-functionalized GO nanofillers (G-P), and the formed interfacial interaction between G-P nanofillers and PBT host promotes the dispersion and compatibility of nanofillers with PBT matrix.

Thereby, a series of PEGMA-functionalized GO nanofillers (G-P) are prepared through the surface polymerization of PEGMA monomer with the catalysis of CAN. By introducing various G-P nanofillers into PBT matrix, thermal stability and mechanical properties of PBT nanocomposites are deeply characterized. Furthermore, the enhancement for thermal stability and mechanical properties of nanocomposites also is analyzed from the aspect of nucleation and crystallization process of PBT matrix influenced by the G-P nanofillers. The effect of anchored PEGMA chains onto GO nanofillers on the PBT matrix is studied in detail from the viewpoint of molecular interaction.

2 Experimental

2.1 Materials

Poly(butylene terephthalate) (PBT, LUPOX-HV1010) used in this study is a commercial product of LG Chem, Korea. Natural graphite powder (NGP) (325 mesh, natural microcrystalline grade, 99%) was purchased from Qingdao Laixi Graphite Co., Ltd. Concentrated sulfuric acid (H_2SO_4, 98%), potassium permanganate ($KMnO_4$), sodium nitrate ($NaNO_3$), hydrochloric acid (HCl, 37%), concentrated nitric acid (HNO_3, 68%) and hydrogen peroxide (H_2O_2, 30%) were provided by Tianjin Guangfu Fine Chemical Industry Institute, and used as received. Polyethylene glycol methacrylate (PEGMA, $M_n = 950$) and ceric ammonium nitrate (CAN) were purchased from Sigma-Aldrich Co. Ltd (Shanghai).

2.2 Preparation of G-P nanofillers

GO was prepared through natural graphite powers according to our previous study [30]. The preparation of PEGMA-functionalized GO nanofillers (G-P) was described as follows. 10 mmol of PEGMA monomer was dropped into GO dispersion (1 mg/mL) under stirring, and subsequently, the CAN solution of nitric acid (1 mol/mL) was slowly dropped. After that, the polymerization process began at 60 °C for 8 h under N_2. The raw suspension was firstly centrifuged, and then washed five times to remove the unreacted monomer or homopolymer. G-P nanofillers were further vacuum-dried at 50 °C before use. Scheme 1 gives the preparation process of G-P nanofillers.

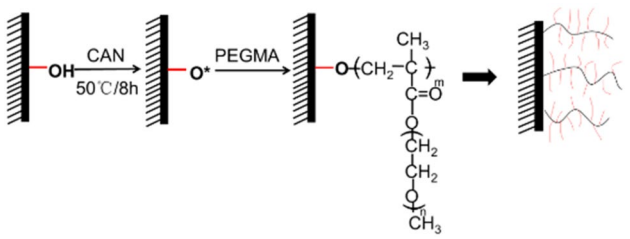

Scheme 1 The redox polymerization of PEGMA onto GO flakes

2.3 Preparation of PBT/G-P nanocomposites

The preparation of PBT/G-P nanocomposites was described as follows. G-P nanofillers were firstly dispersed in a mixed solvent of dichloromethane and trifluoroacetic acid (1:3) via ultrasonication for 3 h to obtain a homogeneous suspension. Then, PBT was slowly dropped into G-P solution under stirring. Subsequently, PBT/G-P mixtures were scratched onto a clean glass plate and then were vacuum-dried at 40 °C until constant mass. The mass fraction, *m*, of G-P in PBT/G-P-*m* composites varied from 0.1 to 3 wt%. Similarly, PBT/GO composites also were fabricated through the same procedure for a comparison.

2.4 Characterization

Fourier transform infrared spectroscopy (FTIR) (Nicolet IS5) at a resolution of 4 cm^{-1} in a wavenumber range from 4000 to 500 cm^{-1}, X-ray powder diffraction (XRD, Bruker D8 DISCOVER) at 40 kV and 150 mA under CuKa radiation ($\lambda = 1.54$ nm), field-emission scanning electron microscopy (FE-SEM, Hitachi S4800, Japan) with an accelerating voltage of 10 kV and X-ray photoelectron spectroscopy (XPS) (GENESIS EDAX, US) with Al Kα radiation ($hv = 1486.4$ eV) are used to analyze the chemical structure and morphology. The tensile testing was carried out on SSANS-20 kN (Shanghai) with a crosshead speed of 5 mm/min at room temperature. Samples were cut into a rectangular sheet, and the tensile properties were obtained by five times average for each sample.

DSC measurements were performed with NETZSCH DSC 200 F3 under N_2 condition. Samples (ca.10.0 mg) were heated to 250 °C and held for 3 min to remove the thermal history. Subsequently, the thermal cycle between 0 and 250 °C was performed at scanning rate of 10 °C/min. The second cycle was used. The isothermal crystallization experiment was performed at 190 °C, and the Avrami equation is used to analyze the crystallization kinetic parameters.

Polarized light microscopy (PLM) (Olympus, BX-51) equipped with a hot-stage (Linkam, THMS600) and digital camera (Micropublisher) was used to analyze the crystal morphology of composites. Specimens were firstly heated to 300 °C and kept for 10 min to remove the thermal history. Temperature was quickly cooled down to 220 °C at a rate of 150 °C/min, and then, the isothermal crystallization experiment was performed.

3 Results and discussion

3.1 Structure identification of G-P nanofillers

FTIR spectra of GO and G-P nanofillers are presented in Fig. 1a. The bands at 3432 cm^{-1}, 1734 cm^{-1}, 1632 cm^{-1}, 1226 cm^{-1} and 1077 cm^{-1}, characteristic of –OH, C=O, –C=C–, C–OH and C–O–C groups, are clearly seen for GO flakes [31, 32]. For G-P nanofillers, similar bands with P(PEGMA) appear at 1453 cm^{-1}, 1265 cm^{-1} and 1100 cm^{-1}, which corresponds to $–CH_3$, C–O–C, C=O groups, respectively [33]. The enhanced 2919 cm^{-1} band ($–CH_2–$) and 1719 cm^{-1} (C=O), as well as the weakened 1625 cm^{-1} (–C=C–) demonstrate the successfully grafting of PEGMA chains onto GO surface. XRD patterns for GO, P(PEGMA) and G-P are shown in Fig. 1b. Clearly, a characteristic diffraction peak at 10.5° for GO flakes appears [34]. Bulk P(PEGMA) shows three crystal diffraction peaks at 19.3, 23.5 and 26.5°, which is ascribed to the crystalline PEG chains. After polymerization of PEGMA onto GO sheets, G-P nanofillers give a down-shifted diffraction peak at 7.2°, illustrating an enhanced *d*-spacing of 1.547 nm against the original 0.842 nm of GO flakes, which is mainly attributed to the incorporated polymer chains. Also, the residual peak at ca. 19.3° further indicates the grafted PEGMA chains onto GO sheets. Meanwhile, from the presented XPS results in Fig. 1c, d, the C/O ratio for G-P nanofillers is 1.86, which is higher than that of GO (1.55). After the curve fitting of C1s spectrum, the proportion of C–O bond from GO and G-P is calculated. A remarkable increased C–O concentration from 23% of GO to 36% of G-P nanofillers further proves that PEGMA has been successfully grafted on GO surface.

3.2 Nucleation influence of G-P nanofillers onto PBT matrix

Typically, the incorporated organic or inorganic nanofillers into polymer matrix show a big effect on the crystallization behavior of polymers. And, a heterogeneous nucleation growth is realized by the incorporated nanofillers [35, 36]. Figure 2 presents the DSC thermograms for PBT/G-P-*m* composites with different contents of G-P nanofillers, where x changes from 0 to 3 wt%, respectively. During the heating and cooling process, the incorporated G-P nanofillers show a great influence on the

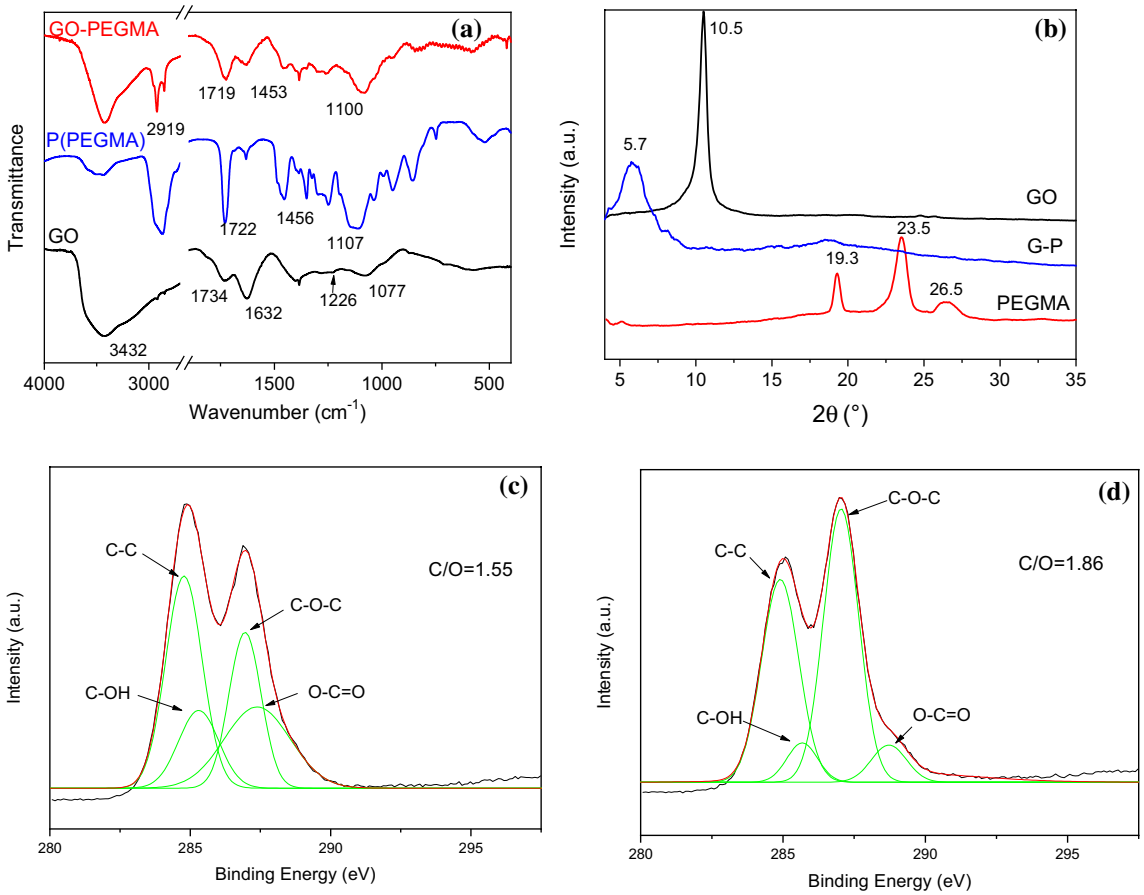

Fig. 1 FTIR spectra **a** and XRD patterns **b** of GO, bulk P(PEGMA) and G-P nanofillers; C1s spectra of XPS results for GO (**c**) and G-P nanofillers (**d**)

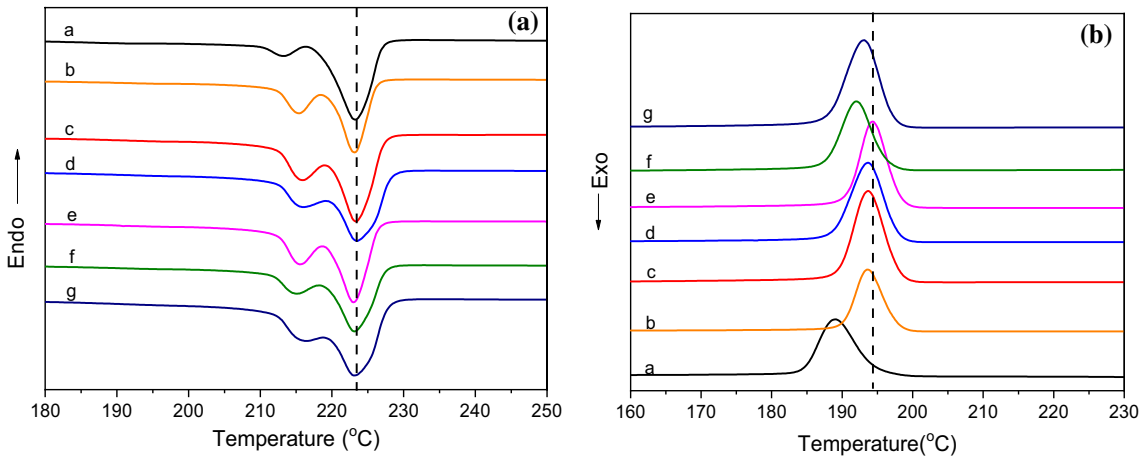

Fig. 2 DSC thermograms of PBT/G-P-*m* nanocomposites with different contents of G-P nanofillers. **a** *m* = 0; **b** 0.1; **c** 0.5; **d** 1.0; **e** 1.5; **f** 2.0; **g** 3.0 wt%

crystallization temperature for PBT/G-P-*m* nanocomposites. The calorimetric data such as the first melting temperature (T_{m1}), the second melting peak (T_{m2}), the onset crystallization temperature (T_{co}), the crystallization peak (T_{cp}) and the endset crystallization temperature (T_{ce}), as well as the melting (ΔH_m) and the cooling enthalpy (ΔH_c) of PBT/G-P-*m* composites are summarized in Table 1. Interestingly, the incorporated G-P nanofillers show a

Table 1 Calorimetric data for PBT/G-P nanocomposites with the varied contents of G-P nanofillers

Samples	G-P (wt%)	ΔH_c (J/g)	T_{cp} (°C)	T_{co} (°C)	T_{ce} (°C)	ΔH_m (J/g)	T_{m1} (°C)	T_{m2} (°C)	X (%)
PBT/G-P	0.0	47.7	189.4	194.7	184.7	41.7	213.2	222.7	29.8
	0.1	49.1	194.1	197.9	190.2	42.5	215.3	222.8	30.3
	0.5	49.4	194.3	198.3	189.7	43.3	215.8	222.9	31.1
	1.0	49.9	194.2	198.0	188.8	45.3	215.8	223.1	32.7
	1.5	50.2	194.9	198.4	190.9	45.8	215.5	222.5	33.2
	2.0	48.4	194.2	197.4	190.2	44.1	215.1	222.6	32.1
	3.0	45.3	193.7	197.4	188.2	41.6	216.2	222.7	30.6

certain effect on T_{m1}, but no effect on T_{m2}, as seen in Fig. 2a and Table 1. T_{m1} presents an increased tendency as compared with the bulk PBT matrix, and with the contents of G-P nanofillers increasing, T_{m1} of composites is 2 °C higher than that of the neat one. The explanations could be ascribed to the melting–recrystallization behavior of PBT lamellae [37]. During the heating–cooling process, the imperfect crystallites composed by PBT chains show a continuous melting–recrystallization process, and then, the crystal size gives a thickened behavior. Note that, however, T_{m2} does not present an obvious change with the increased G-P nanofillers. This preliminary implies that the introduced G-P nanofillers do not alter the crystal structure of PBT matrix.

A different variation for the crystallization process from the melting process is well shown, as illustrated in Fig. 2b. The incorporated G-P nanofillers contribute higher T_{cp}, T_{co} and T_{ce} of PBT/G-P-*m* nanocomposites than that of the neat one. Almost, an increment for T_{cp}, T_{co} and T_{ce} is seen as the G-P nanofillers increase from 0.1 to 3.0 wt%, showing a good nucleation ability. Accordingly, a maximum 5.5 °C for T_{cp} and 6.2 °C for T_{ce} is found at 1.5 wt% G-P nanofillers. This is mainly attributed to the heterogeneous nucleation role of G-P nanofillers to PBT matrix. Considering the large aspect ratio of GO sheets and the similar PEGMA chains with PBT matrix, the molecular interaction and the crystallization ability of PBT matrix are greatly enhanced. Moreover, the anchored PEGMA chains also improve the interfacial compatibility between GO nanosheets and PBT matrix, offering a good dispersion behavior. To give a description to the crystallization of PBT influenced by G-P nanofillers, crystallinity (X) is calculated through the following Eq. (1) [38].

$$x = \frac{\Delta H_m}{w \Delta H_m^0} \times 100\% \quad (1)$$

where ΔH_m is the experimental melting enthalpy of PBT nanocomposites, $\Delta H_m^0 = 140$ J/g [39] represents the neat PBT, and W is the mass fraction of PBT.

It can be seen that the crystallinity, X, increases first to 33.2% at 1.5 wt% G-P nanofillers and then decreases to 30.6% at 3.0 wt% loadings. As compared with neat PBT, the introduced G-P nanofillers effectively promote the crystallization behavior of PBT nanocomposites. In addition, if the overloaded G-P nanofillers are used, their aggregation state is seen, which leads to the decreased ordered stacking state of PBT chains. So, the introduced G-P nanofillers into PBT matrix should below 1.5 wt% to obtain a good dispersion according to DSC results. In general, the incorporated G-P nanofillers play a heterogeneous nucleation role and also promote the crystallization behavior of PBT matrix at low content, as compared with the neat one.

X-ray diffraction technique is used to probe the crystal structure of PBT/G-P-*m* nanocomposites at room temperature. As shown in Fig. 3, neat PBT presents the obvious diffraction peaks at 16.2°, 17.3°, 20.7°, 23.4° and 25.3°, corresponding to [011], [010], [110], [100] and [111] plane, which characterizes α-crystal structure. Clearly, PBT/G-P nanocomposites also exhibit a similar one with that of neat PBT, and these diffraction peaks basically keep constant regardless of the varied contents of G-P nanofillers. This indicates that the incorporated G-P nanofillers do not alter the crystal structure of PBT

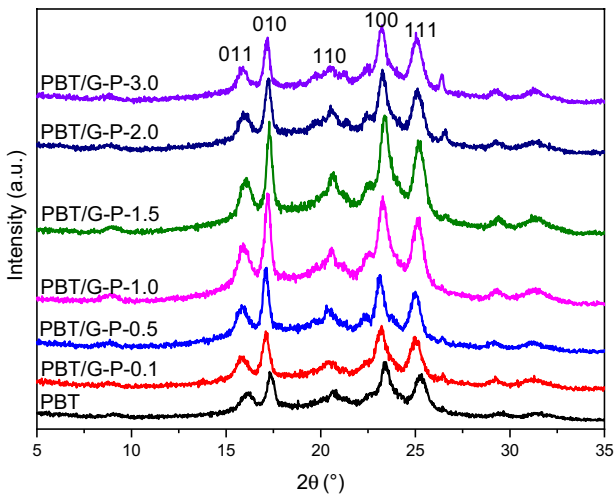

Fig. 3 XRD patterns of PBT and PBT/G-P-*m* nanocomposites

matrix. Through Scherrer equation (Eq. 2), the crystallite size of PBT is calculated, and they are summarized in Table 2.

$$L_{hkl} = \frac{K\lambda}{\beta_{hkl}\cos\theta_{hkl}} \quad (2)$$

where L_{hkl} is the crystallite size, characterizing [*hkl*] plane; K is the Scherrer constant and $K = 0.9$ is used. β_{hkl} is the width at half height; λ is X-ray wavelength; θ is the Bragg angle.

From the compared results shown in Table 2, the crystallite dimensions of PBT/G-P-*m* nanocomposites are smaller than those of neat PBT. In contrast to the slight decrease in the [011] and [100] planes, a remarkable decreased L_{hkl} corresponding to the [010], indicating the preferred growth plane of a lamellae growth direction, is observed on the PBT/G-P nanocomposites. It indicates that the incorporated G-P nanofillers have a strong nucleation effect on the crystallization of PBT matrix. The increased heterogeneous nucleation sites from G-P nanofillers affect the growth of PBT crystal, and thus, the adjacent spherulitic morphology is destroyed during the growth process.

Table 2 Crystallite size of PBT/G-P-*m* nanocomposites with varied contents of G-P nanofillers

Samples	G-P (wt%)	L_{hkl} (nm)				
		[011]	[010]	[110]	[100]	[111]
PBT/G-P	0	7.9	20.8	4.1	10.6	10.3
	0.1	7.7	18.1	3.3	9.7	10.0
	0.5	7.5	17.3	3.5	9.5	9.5
	1.0	7.2	16.1	4.2	9.1	8.7
	1.5	6.7	15.4	3.5	8.8	8.3
	2.0	6.8	15.1	3.3	8.7	8.3
	3.0	6.7	14.8	3.1	8.8	8.1

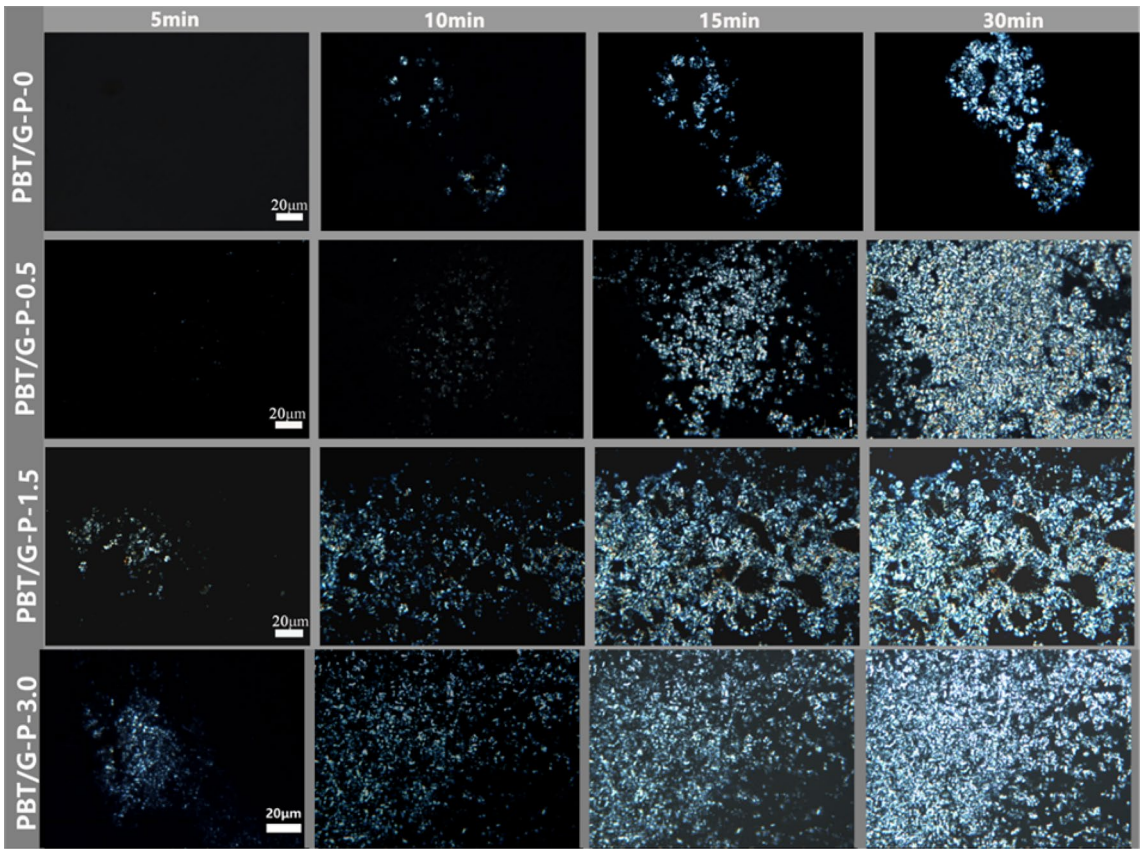

Fig. 4 PLM picture of PBT/G-P-*m* nanocomposites with varied G-P nanofillers

In light of the heterogeneous nucleation role of G-P nanofillers to PBT matrix, the crystal morphology observed by PLM is illustrated in Fig. 4. After isothermal crystallization at 220 °C for the different time, PBT and its nanocomposite give the different crystal morphology owing to the influence of G-P nanofillers. Generally, spherulitic crystal morphology is not well seen for PBT matrix regardless of the existence of G-P nanofillers or not [15]. It can be seen that PBT gives the lower crystal number than that of PBT/G-P nanocomposites. For PBT matrix, the crystal morphology appears up to 10 min, and with the isothermal crystallization time further increasing to 30 min, the crystal number shows an increase followed by an unchanged crystal size. On the contrary, PBT/G-P-*m* nanocomposites give a different picture based on the incorporated amount of G-P nanofillers. With the content of G-P nanofillers changing from 0.5 to 3.0 wt%, the crystal number shows first an increasing tendency. This is due to the nucleation contribution of G-P nanofillers, and the enhanced nucleation sites of PBT chain [40]. However, an overloaded content could block the crystallization ability of PBT matrix and limit the packing manner of molecular chains. This is well supported from the DSC results, and the crystallinity presents a decreased behavior at 3.0 wt% as compared with at 1.5 wt%. Therefore, it is highly suggested that the incorporated G-P nanofillers effectively promote the crystallization of PBT matrix with the content below 1.5 wt%. In the meantime, PBT/G-P-1.5 shows a maximum crystal growth rate and crystallinity, and the nucleation density rapidly increases against the others. In addition, it is worthy to note that the crystallinity of PBT is very low although the G-P nanofillers are helpful to promote the crystallization behavior of PBT matrix based on PLM and DSC results. Then, spherulites sizes are too small to be clearly distinguished by PLM. This phenomenon is similar to the study of Wu et al. [15], who also does not observe the nucleation of PBT influenced by CNTs through PLM. However, the incorporated CNTs give a higher crystallinity than that of the G-P nanofillers. Probably, the nanofillers' size and morphology, and the molecular weight of PBT show the different contribution to the crystallinity of PBT chains.

In order to understand the crystallization behavior and the morphology obtained by PLM, the isothermal crystallization experiment of PBT/G-P-*m* nanocomposites is performed, and the isothermal crystallization data are summarized in Table 3. Clearly, PBT/G-P nanocomposites exhibit a decreased Avrami exponent (*n*) than that of neat PBT, indicating that the incorporated G-P nanofillers influence the crystallization behavior of PBT matrix. From the varied crystallization rate constant (*K*) and $t_{1/2}$, it can be concluded that the G-P nanofillers effectively promote the crystallization process of PBT matrix, illustrating a heterogeneous nucleation role. $t_{1/2}$ reaches a minimum one, and the crystallinity (X_c) gets a maximum one at 1.5 wt% of G-P nanofillers. Further increasing G-P nanofillers to 3.0 wt%, X_c begins to decrease, followed by an increased $t_{1/2}$ value, confirming the overloaded G-P nanofillers play a negative influence on the crystallization process of PBT matrix. This result is good agreement with that of PLM, demonstrating the heterogeneous nucleation role of G-P nanofillers to PBT matrix.

Table 3 Isothermal crystallization parameters for PBT and PBT/G-P nanocomposites

Samples	*n*	*K*	$t_{1/2}$/s	X_c/%
PBT	2.7	3.6	26.3	28.9
PBT/G-P-0.5	1.8	11.0	15.0	30.9
PBT/G-P-1.5	1.6	14.9	12.9	32.7
PBT/G-P-3.0	1.9	3.9	18.1	29.7

*K is the crystallization rate constant; n is the Avrami exponent; $t_{1/2}$ is the half-time to reach 50% crystallinity; X_c is the crystallinity

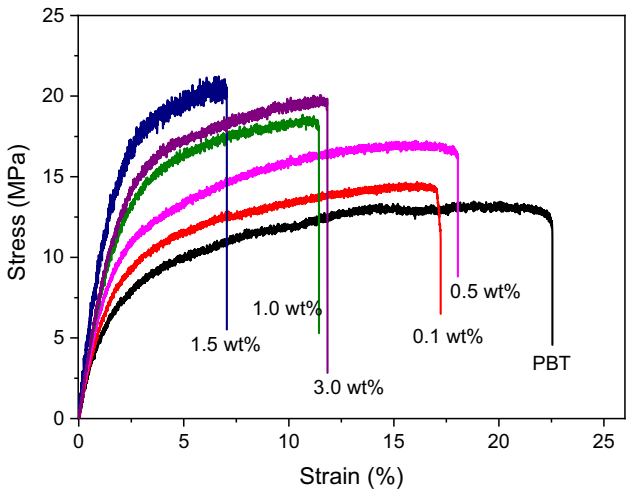

Fig. 5 Stress–strain curves of PBT and PBT/G-P-*m* nanocomposites with the different contents of G-P nanofillers

3.3 Mechanical properties of PBT/G-P nanocomposites

Tensile measurements are performed for PBT and PBT/G-P nanocomposites to clarify the effect of G-P nanofillers on the mechanical property of PBT matrix. Figure 5 presents the typical stress–strain curves for these nanocomposites. Clearly, neat PBT exhibits the lowest stress value than that of PBT/G-P nanocomposites, showing an extensive deformation with a yield strength region. For PBT/G-P nanocomposites, the mechanical performance strongly depends on the content of nanofillers [41]. With the loading of

G-P nanofillers increasing from 0.1 to 1.5 wt%, the yield stress increases accompanied by a decreased yield strain. At 1.5 wt% G-P nanofillers, the yield strength reaches the maximum one among PBT/G-P-*m* nanocomposites. The high yield strength of PBT nanocomposites is originated from the incorporated G-P nanofillers, increasing the interfacial stress-transfer process of PBT matrix. In the meantime, the grafted PEGMA chains onto GO surface also promote the interfacial compatibility between PBT and GO flakes, contributing an increase in the yield strength of PBT matrix. However, further increasing G-P nanofillers to 3.0 wt%, the yield strength decreases, which is also higher than that of neat PBT. This indicates that the overloaded nanofillers present an aggregated behavior, and then, the dispersion into PBT matrix is greatly decreased.

To give an understanding of the interfacial interaction between nanofillers and PBT matrix, a comparison for the tensile strength and modulus is presented in Fig. 6. Clearly, neat PBT gives a lower tensile strength (13.5 MPa) and modulus (378 MPa) as compared with PBT/G-P and PBT/GO nanocomposites. From the compared results, tensile strength and tensile modulus exhibit an increased tendency with the incorporated amount of G-P and GO nanofillers. And, at the low contents, this enhancement is very sensitive, and a quick increase is found below 0.5 wt% regardless of the type of nanofillers. Interestingly, PBT/GO nanocomposites give a tensile modulus (609 MPa) and strength (17.2 MPa) at 0.5 wt% GO; however, PBT/G-P nanocomposites reach to 626 MPa (tensile modulus) and 17.4 MPa (tensile strength), respectively. Slightly improved tensile properties are seen for PBT/G-P nanocomposites when the G-P nanofillers grafted by PEGMA chains are incorporated as compared with GO nanofillers. This further demonstrates that the interfacial compatibility gets strong after the GO surface is modified. Accordingly, further up

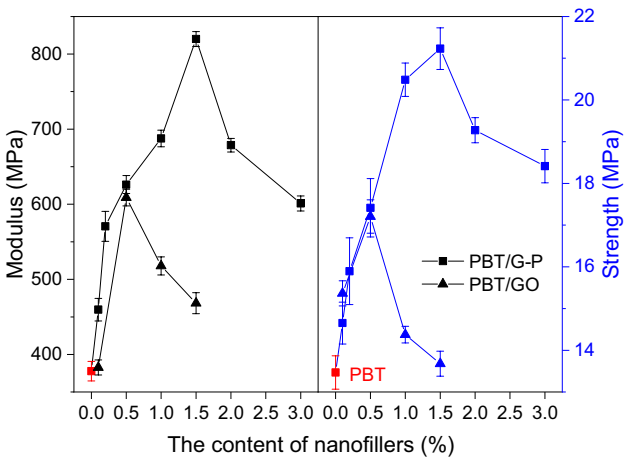

Fig. 6 Compared tensile strength and modulus of PBT nanocomposites with different contents of G-P and GO nanofillers

increasing GO contents to 1.5 wt%, PBT/GO nanocomposites give a decreased tensile strength (13.7 MPa) and modulus (468 MPa). On the contrary, PBT/G-P nanocomposites reach the maximum (820 MPa for modulus and 21.2 MPa for strength) at 1.5 wt% G-P nanofillers. Such a comparison demonstrates that the surface-modified GO by PEGMA chains is beneficial to enhance the mechanical properties of PBT matrix. And, the incorporated amount for the surface-modified GO is far above the untreated one because of the enhanced compatibility with PBT matrix [23, 42]. However, when the content of G-P nanofillers increases to 3.0 wt%, tensile strength and modulus decrease to 18.4 MPa and 601 MPa, respectively. This could be attributed to the overloaded G-P nanofillers, leading to an aggregation in PBT matrix. Although the decreased mechanical properties at high content of G-P nanofillers are demonstrated in Fig. 5, the enhanced amplitude of tensile strength and modulus is much higher than that of neat PBT and PBT/GO nanocomposites. This illustrates that the compatibility and the interfacial interaction are helpful to promote the stress transfer from the nanofillers to the matrix [43, 44]. Therefore, this enhanced performance for PBT/G-P nanocomposites also supports the nucleation behavior of G-P nanofillers, as illustrated in Fig. 4 and Table 3. The enhanced crystallization behavior of PBT matrix contributes the stress-transfer process in light of the increased heterogeneous nucleation sites and the thickened interfacial layers influenced from the G-P nanofillers [8]. Although the overloaded G-P nanofillers (3.0 wt%) provide much more nucleation sites to PBT matrix, they exhibit an aggregated phenomenon, which results in a decreased tensile property. Given that the nucleation density is beyond a critical concentration, the structural unity and the chain rearrangement of PBT nanocomposites are destroyed, and then, the enhanced tensile properties are prohibited [7]. So, the nucleation density of PBT matrix originated from G-P nanofillers demonstrates an important influence on the mechanical properties of nanocomposites.

Table 4 summarizes the varied tensile modulus and strength for PBT nanocomposites with different nanofillers. From the presented results, it can be seen that the incorporated nanofillers show an enhanced mechanical property for PBT matrix. And, the increased tensile modulus and strength is highly depended upon the nanofillers' contents, as compared with neat PBT. Interestingly, for the untreated nanofillers, a smaller increment in tensile modulus and strength is indicated under a higher loading of CNT-based nanofillers [7]. Moreover, the high content of CNT-based nanofillers inevitable blocks the formation of stress-transfer network for PBT matrix. After introducing the surface-modified CNT nanofillers (PBT-g-MWCNT), the higher tensile modulus and strength than the untreated

Table 4 Compared tensile modulus and strength for PBT nanocomposites influenced by the varied nanofillers

Nanofillers	Increased tensile modulus, %	Increased tensile strength, %	Method	Reference
1.0 wt% oSWCNT	14	29	In situ polymerization	[6]
2.0 wt% CNT	22	35	Melt blending	[7]
3.0 wt% MWCNT	38	25		[42]
3.0 wt% PBT-g-MWCNT	46	42		
0.5 wt% GO	61	28	Solution blending	This work
1.5 wt% G-P	117	58		

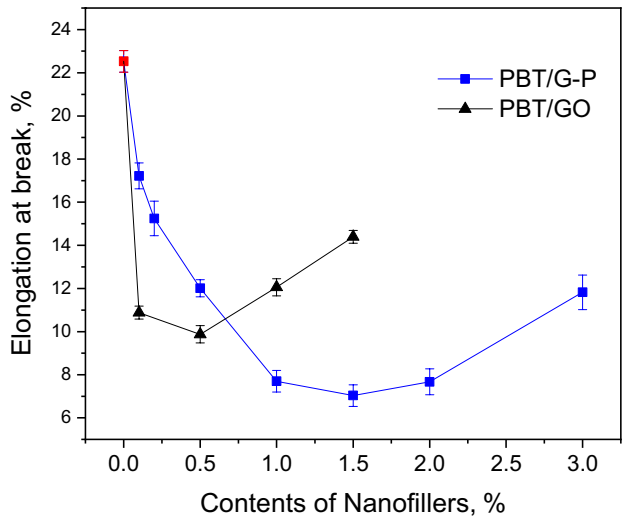

Fig. 7 Elongation at break of PBT nanocomposites influenced by GO and G-P nanofillers

one is demonstrated [42]. This explains that the surface-functionalized nanofillers bring an enhanced interfacial transfer behavior. And, our present results also support this finding. Note that, the PEGMA-modified GO (G-P) nanofillers give an obvious increment in tensile modulus and strength against the pristine GO, and the maximum loadings for these two nanofillers are different because of their varied dispersion ability in PBT matrix. In addition, CNT- and GO-based nanofillers show the different influence on the mechanical properties of PBT matrix, and this influence from the morphology and the aspect ratio need to be analyzed including the interfacial state, the dispersion and the compatibility, as well as the orientation for nanofillers.

Figure 7 gives the compared elongation at break of PBT nanocomposites under the influence of GO and G-P nanofillers. Clearly, the influence of GO and G-P nanofillers is different for PBT nanocomposites. Both PBT/GO and PBT/G-P nanocomposites give the smallest elongation at break at the maximum tensile modulus and strength. This indicates that the incorporated nanofillers decrease the ductility of PBT matrix and increase the matrix stiffness [20]. The elongation at break for PBT shows first a decrement with the content increasing to 0.5 and 1.5 wt% for GO and G-P nanofillers, respectively, and then continues to increase beyond this concentration. Such an increased elongation indicates that the interfacial compatibility and dispersion of nanofillers in PBT matrix decreases, resulting in a limited stress-transfer network. Note that, the incorporated G-P nanofillers offer an increased mechanical property, but the ductility shows a decrement, as compared with GO nanofillers. Therefore, the balance between stiffness and ductility should be considered, and an optimal content is important for the formation of interfacial layer and the stress-transfer network.

3.4 Morphology of PBT/G-P nanocomposites

The good dispersion of nanofillers into polymer matrix is important to realize high-performance nanocomposites [45, 46]. Figure 8 illustrates the morphology of PBT/G-P-*m* nanocomposites with different contents of G-P nanofillers. A uniform and smooth fracture is found for neat PBT, while for PBT/G-P nanocomposites, a rough and wrinkled image can be seen. With the G-P nanofillers increasing, the roughness of fracture shows more and more obvious, and some aggregated nanofillers are found. Note that, no aggregation appears when the 1.5 wt% G-P nanofillers are introduced. This demonstrates that the surface-modified GO nanofillers effectively improve the interfacial compatibility with PBT matrix [47]. And so, the dispersion is greatly enhanced due to the interaction between the PEGMA chain and PBT matrix. Further increasing G-P nanofillers to 3 wt%, an obvious aggregated state is shown, and then, the dispersion decreases. Such a varied morphology also supports the findings of mechanical properties of PBT/G-P nanocomposites. That is to say, the incorporated nanofillers into PBT matrix exist a critical content, and the stress-transfer network composed of G-P nanofillers and PBT matrix shows good advantage over the neat one. Thus, the chain entanglement between PEGMA and PBT promotes the nucleation, crystallization behavior and the mechanical properties based on the good dispersion and interfacial interaction. The present study preliminary demonstrates

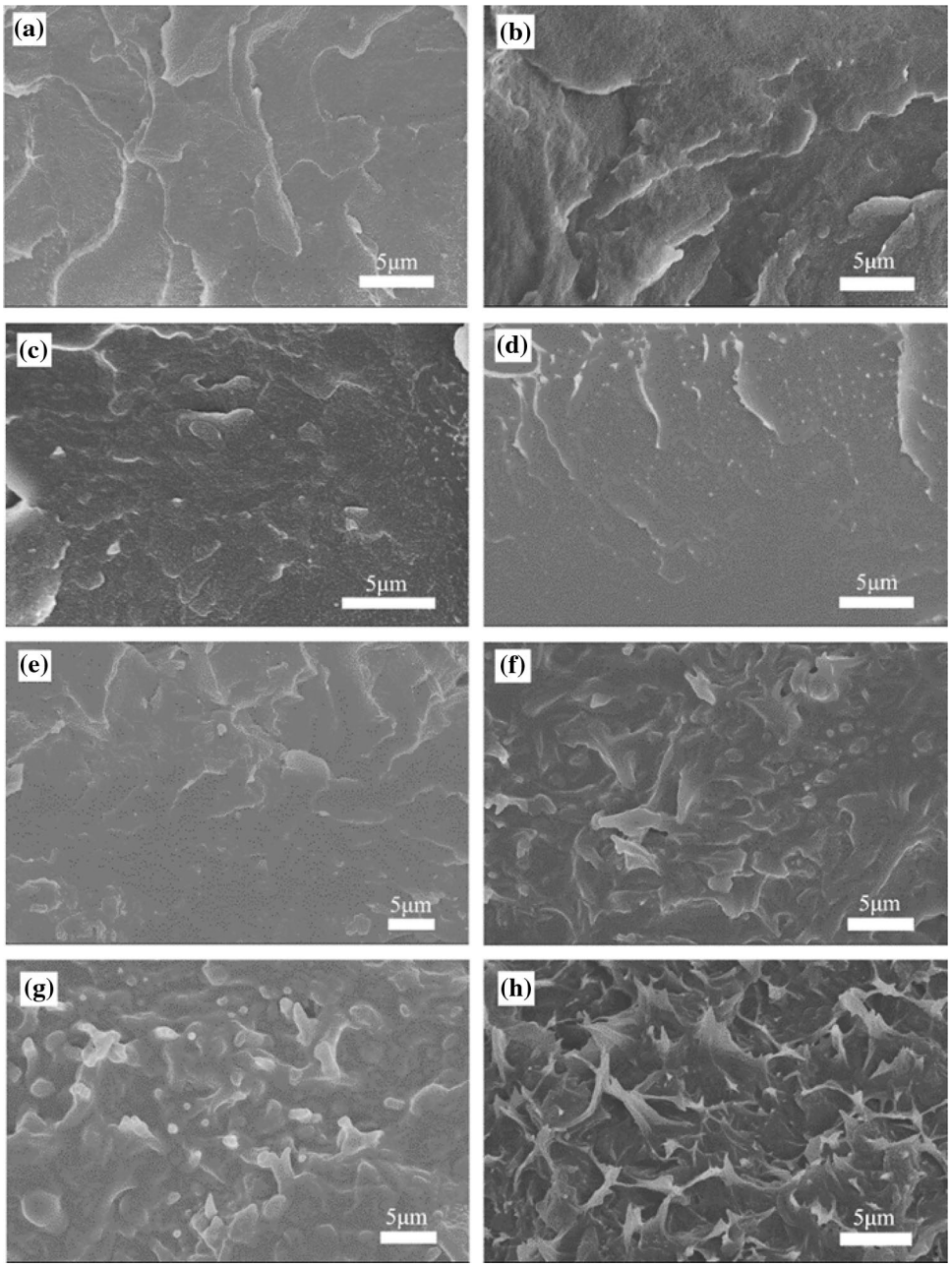

Fig. 8 SEM images of PBT/G-P-*m* nanocomposites with various G-P contents. **a** PBT, **b** 0.1, **c** 0.5, **d** 1.0, **e** 1.5, **f** 2.0, **g** 3.0 wt%

that the enhanced interfacial layer and nucleation behavior is helpful to PBT nanocomposites offering an increased mechanical performance.

4 Conclusion

In this paper, a series of PBT/G-P nanocomposites with varied contents of G-P nanofillers, prepared from the surface-initiated polymerization of polyethylene glycol methacrylate onto GO surface under the catalysis of ceric ammonium nitrate, are fabricated through a solution-blending technique. The incorporated G-P nanofillers induce the enhanced nucleation sites and crystallinity for PBT matrix based on their heterogeneous nucleation role. The interfacial interaction between G-P nanofillers and PBT matrix contributes a good dispersion, and the enhanced mechanical properties are originated from the formed stress-transfer network. At 1.5 wt% loading, PBT/G-P nanocomposites give a maximum mechanical property, followed by 58% and 117% increase in the tensile strength and modulus, respectively, as compared with neat one. Good dispersion and strong interfacial interaction from G-P nanofillers and PBT matrix are important for the preparation of high-performance nanocomposites. Therefore, the present study demonstrates that the enhanced

interfacial layer and nucleation behavior is helpful to PBT nanocomposites showing an increased mechanical performance.

Acknowledgements This work was funded by National Natural Science Foundation of China (21875163), National Key R&D Program of China (2017YFB0309100) and Key Project of Tianjin Municipal Natural Science Foundation (16JCZDJC37000).

Compliance with ethical standards

Conflict of interest The authors declare that they have no conflict of interest.

References

1. Yokouchi M, Sakakibara Y, Chatani Y, Tadokoro H, Tanaka T, Yoda K (1976) Structures of two crystalline forms of poly(butylene terephthalate) and reversible transition between them by mechanical deformation. Macromolecules 9(2):266–273
2. Hobbs SY, Pratt CF (2010) The effect of skin-core morphology on the impact fracture of poly(butylene terephthalate). J Appl Polym Sci 19(6):1701–1722
3. Hobbs SY, Bopp RC (1980) Fracture toughness of poly(butylene terephthalate). Polymer 21(5):559–563
4. Gensler R, Gröppel P, Muhrer V, Müller N (2015) Application of nanoparticles in polymers for electronics and electrical engineering. Part Part Syst Charact 19(5):293–299
5. Acierno D, Scarfato P, Amendola E, Nocerino G, Costa G (2010) Preparation and characterization of PBT nanocomposites compounded with different montmorillonites. Polym Eng Sci 44(6):1012–1018
6. Broza G, Kwiatkowska M, Rosłaniec Z, Schulte K (2005) Processing and assessment of poly(butylene terephthalate) nanocomposites reinforced with oxidized single wall carbon nanotubes. Polymer 46(16):5860–5867
7. Kim JY (2010) The effect of carbon nanotube on the physical properties of poly(butylene terephthalate) nanocomposite by simple melt blending. J Appl Polym Sci 112(5):2589–2600
8. Chopra S, Deshmukh KA, Peshwe D (2017) Theoretical prediction of interfacial properties of PBT/CNT nanocomposites and its experimental evaluation. Mech Mater 109:11–17
9. Aróstegui A, Nazábal J (2003) Stiffer and super-tough poly(butylene terephthalate) based blends by modification with phenoxy and maleated poly(ethylene-octene) copolymers. Polymer 44(1):239–249
10. Hwang SS (2016) Tensile, electrical conductivity and EMI shielding properties of solid and foamed PBT/carbon fiber composites. Compos B Eng 98:1–8
11. Deshmukh GS, Peshwe DR, Pathak SU, Ekhe JD (2014) Nonisothermal crystallization kinetics and melting behavior of poly(butylene terephthalate) (PBT) composites based on different types of functional fillers. Thermochim Acta 581(6):41–53
12. Che J, Luan B, Yang X, Lu L, Wang X (2005) Graft polymerization onto nano-sized SiO_2 surface and its application to the modification of PBT. Mater Lett 59(13):1603–1609
13. Chang JH, An YU, Kim SJ, Im S (2003) Poly(butylene terephthalate)/organoclay nanocomposites prepared by in situ interlayer polymerization and its fiber (II). Polymer 44(19):5655–5661
14. Ercan N, Oburoğlu N, Kaşgöz A, Durmus A (2012) Effects of halloysite nanotube on the mechanical properties and nonisothermal crystallization kinetics of poly(butylene terephthalate) (PBT). J Macromol Sci Part B 51(5):860–879
15. Wu D, Wu L, Yu G, Xu B, Zhang M (2010) Crystallization and thermal behavior of multiwalled carbon nanotube/poly(butylenes terephthalate) composites. Polym Eng Sci 48(6):1057–1067
16. Huang T, Li JL, Yang JH, Zhang N, Wang Y, Zhou ZW (2018) Carbon nanotubes induced microstructure and property changes of polycarbonate/poly(butylene terephthalate) blend. Compos B Eng 133:177–184
17. Espinoza-Martinez A, Avila-Orta C, Cruz-Delgado V, Olvera-Neria O, Gonzalez-Torres J, Medellin-Rodriguez F (2012) Nucleation mechanisms of aromatic polyesters, PET, PBT, and PEN, on single-wall carbon nanotubes: early nucleation stages. J Nanomater 2012:10. https://doi.org/10.1155/2012/189820
18. Tallury SS, Pasquinelli MA (2010) Molecular dynamics simulations of polymers with stiff backbones interacting with single-walled carbon nanotubes. J Phys Chem B 114(29):9349–9355
19. Li M, Jeong YG (2012) Influences of exfoliated graphite on structures, thermal stability, mechanical modulus, and electrical resistivity of poly(butylene terephthalate). J Appl Polym Sci 125(S1):E532–E540
20. Bian J, Lin HL, He FX, Wang L, Wei XW, Chang IT, Sancaktar E (2013) Processing and assessment of high-performance poly(butylene terephthalate) nanocomposites reinforced with microwave exfoliated graphite oxide nanosheets. Eur Polym J 49(6):1406–1423
21. Liu L, Barber AH, Nuriel S, Wagner HD (2005) Mechanical properties of functionalized single-walled carbon-nanotube/poly(vinyl alcohol) nanocomposites. Adv Func Mater 15(6):975–980
22. Wei Y, Yang B, Lu H, Lei S, Yuan H (2014) Effect of modified carbon nanotube on the thermal behavior, flame retardancy and mechanical properties of poly(1,4-butylene terephthalate)/aluminum phosphinate composites. Ind Eng Chem Res 53(48):18489–18496
23. Wu CS, Liao HT (2015) Preparation and characterization of functionalized graphite/poly(butylene terephthalate) composites. Polym Bull 72(7):1799–1816
24. Li W, Tang XZ, Zhang HB, Jiang ZG, Yu ZZ, Du XS, Mai YW (2011) Simultaneous surface functionalization and reduction of graphene oxide with octadecylamine for electrically conductive polystyrene composites. Carbon 49(14):4724–4730
25. Chisholm BJ, Moore RB, Barber G, Khouri F, Hempstead A, Larsen M, Olson E, Kelley J, Balch G, Caraher J (2002) Nanocomposites derived from sulfonated poly(butylene terephthalate). Macromolecules 35(14):5508–5516
26. Iulianelli A, Basile A (2012) Sulfonated PEEK-based polymers in PEMFC and DMFC applications: a review. Int J Hydrog Energy 37(20):15241–15255
27. Colonna S, Pérez-Camargo R, Chen H, Liu G, Wang D, Müller A, Saracco G, Fina A (2017) Supernucleation and orientation of poly(butylene terephthalate) crystals in nanocomposites containing highly reduced graphene oxide. Macromolecules 50(23):9380–9393
28. Cao L, Sun Q, Wang H, Zhang X, Shi H (2015) Enhanced stress transfer and thermal properties of polyimide composites with covalent functionalized reduced graphene oxide. Compos A Appl Sci Manuf 68:140–148
29. Zhang L, Jiao H, Jiu H, Chang J, Zhang S, Zhao Y (2016) Thermal, mechanical and electrical properties of polyurethane/(3-aminopropyl) triethoxysilane functionalized graphene/epoxy resin interpenetrating shape memory polymer composites. Compos A Appl Sci Manuf 90:286–295
30. Li S, Kong L, Wang H, Xu H, Li J, Shi H (2018) Thermal performance and shape-stabilization of comb-like polymeric phase change materials enhanced by octadecylamine-functionalized graphene oxide. Energy Convers Manag 168:119–127

31. Si Y, Samulski ET (2008) Synthesis of water soluble graphene. Nano Lett 8(6):1679–1682
32. Pham VH, Cuong TV, Hur SH, Oh E, Kim EJ, Shin EW, Jin SC (2011) Chemical functionalization of graphene sheets by solvothermal reduction of a graphene oxide suspension in N-methyl-2-pyrrolidone. J Mater Chem 21(10):3371–3377
33. Wang H, Lu X, Lu X, Wang Z, Ma J, Wang P (2017) Improved surface hydrophilicity and antifouling property of polysulfone ultrafiltration membrane with poly(ethylene glycol) methyl ether methacrylate grafted graphene oxide nanofillers. Appl Surf Sci 425:603–613
34. Perera SD, Mariano RG, Nijem N, Chabal Y, Ferraris JP Jr, Balkus KJ (2012) Alkaline deoxygenated graphene oxide for supercapacitor applications: an effective green alternative for chemically reduced graphene. J Power Sources 2(10):4498–4506
35. Xu JZ, Zhang ZJ, Xu H, Chen JB, Ran R, Li ZM (2015) Highly enhanced crystallization kinetics of poly(L-lactic acid) by poly(ethylene glycol) grafted graphene oxide simultaneously as heterogeneous nucleation agent and chain mobility promoter. Macromolecules 48(14):4891–4900
36. Ryu SH, Shanmugharaj AM (2014) Influence of hexamethylene diamine functionalized graphene oxide on the melt crystallization and properties of polypropylene nanocomposites. Mater Chem Phys 146(3):478–486
37. Xiao J, Hu Y, Wang Z, Tang Y, Chen Z, Fan W (2005) Preparation and characterization of poly(butylene terephthalate) nanocomposites from thermally stable organic-modified montmorillonite. Eur Polym J 41(5):1030–1035
38. Liu Z, Maréchal P, Jérôme R (1997) DMA and DSC investigations of the β transition of poly(vinylidene fluoride). Polymer 38(19):4925–4929
39. Illers KH (1980) Heat of fusion and specific volume of poly(ethylene terephthalate) and poly(butylene terephthalate. Colloid Polym Sci 258(2):117–124
40. Samthong C, Deetuam C, Yamaguchi M, Praserthdam P, Somwangthanaroj A (2016) Effects of size and shape of dispersed poly(butylene terephthalate) on isothermal crystallization kinetics and morphology of poly(lactic acid) blends. Polym Eng Sci 56(3):258–268
41. Liang J, Huang Y, Zhang L, Wang Y, Ma Y, Guo T, Chen Y (2010) Molecular-level dispersion of graphene into poly(vinyl alcohol) and effective reinforcement of their nanocomposites. Adv Funct Mater 19(14):2297–2302
42. Choi EY, Kim SW, Kim CK (2016) In situ grafting of polybutylene terephthalate onto multi-walled carbon nanotubes by melt extrusion, and characteristics of their composites with polybutylene terephthalate. Compos Sci Technol 132:101–107
43. Xie L, Duan G, Wang W, Wang M, Wu Q, Zhou X, Ge X (2016) Effect of γ-ray-radiation-modified graphene oxide on the integrated mechanical properties of PET blends. Ind Eng Chem Res 55(29):8123–8132
44. Martin-Gallego M, Bernal MM, Hernandez M, Verdejo R, Lopez-Manchado MA (2013) Comparison of filler percolation and mechanical properties in graphene and carbon nanotubes filled epoxy nanocomposites. Eur Polym J 49(6):1347–1353
45. Chiou KC, Chang FC (2015) Reactive compatibilization of polyamide-6 (PA 6)/polybutylene terephthalate (PBT) blends by a multifunctional epoxy resin. J Polym Sci Part B Polym Phys 38(1):23–33
46. Fabbri P, Bassoli E, Bon SB, Valentini L (2012) Preparation and characterization of poly (butylene terephthalate)/graphene composites by in situ polymerization of cyclic butylene terephthalate. Polymer 53(4):897–902
47. Chen Y, Wang X, Wu D (2013) Recycled carbon fiber reinforced poly(butylene terephthalate) thermoplastic composites: fabrication, crystallization behaviors and performance evaluation. Polym Adv Technol 24(4):364–375

Publisher's Note Springer Nature remains neutral with regard to jurisdictional claims in published maps and institutional affiliations.